Research on Engineering Structures & Materials
www.jresm.org
Research Group

*Research Article*

# Design, steady-state optimization, and cascade dynamic control of a continuous four-columns vacuum distillation process for coal tar-derived mixed phenols

Yongli Zheng [*,a]

*School of Biological and Environmental Engineering, Tianjin Vocational University, China*

**Article Info**

***Article History:***

Received 16 July 2026

Accepted 04 Sep 2026

***Keywords:***

Coal tar-derived mixed phenols;
Four-columns vacuum distillation;
NRTL-HOC model;
Cascade control with feedforward compensation;
Total annual cost (TAC)

**Abstract**

Mixed phenolic homologues derived from coal tar, characterized by close boiling points and high thermal sensitivity, exhibit poor separation efficiency and thermal degradation in traditional atmospheric distillation processes. This study designs a continuous four-columns vacuum distillation process. The NRTL-HOC thermodynamic model is selected to rigorously describe the liquid-phase non-ideality and vapor-phase association of polar phenolic molecules. A separation sequence comprising a phenol column, an o-cresol column, an m-/p-cresol mixed-fraction column, and a xylenols column is constructed. The theoretical stages, reflux ratios, and feed locations are optimized by steady-state simulation to minimize energy consumption and total annual cost while satisfying purity and recovery constraints. Considering the strong coupling and large time delays, a temperature-concentration cascade control system with feedforward compensation is designed. Phenol, o-cresol, the m-/p-cresol mixed fraction, and xylenols achieved purities of 99.8%, 99.5%, 99.2%, and 99.0%, with recoveries of 99.1%, 98.7%, 98.2%, and 97.5%, respectively. The total reboiler duty of the four-columns system was 5686.7 kW. Under feed-flow disturbances of ±10% and feed-composition disturbances of ±5%, product purity was restored within 80 min, with a maximum deviation of no more than 0.15%. At 18.0 kPa, the optimized four-columns process achieved a maximum annual net economic margin of USD 1.585 million.



## 1. Introduction

Coal tar, as an important byproduct of the coal chemical industry, contains extremely rich basic chemical raw materials. Phenolic compounds, including phenol, o-cresol, m-/p-cresol, and xylenols, are high-value fine-chemical intermediates widely used in resins, pharmaceuticals, pesticides, and flame retardants [1-2]. How to convert the extremely complex coal tar mixed phenols into high-purity monomer products is not only the core link to improve the overall economic benefits of the coal chemical industry chain, but also the only way to improve the efficiency of resource recycling [3]. However, the efficient separation of coal tar mixed phenols faces great technical challenges in chemical separation engineering. The boiling points of phenolic homologues are close, and the relative volatility of m-cresol to p-cresol is approximately 1.02, making conventional distillation difficult. There are strong polar interactions and highly non-ideal vapor-liquid phase equilibrium characteristics in the system. Meanwhile, phenolic substances are typical heat-sensitive materials, which are prone to oxidation, discoloration, and condensation reactions in high-temperature environments [4-5]. Therefore, the key issue of this system is not simply increasing the number of separation stages, but simultaneously balancing phase-equilibrium prediction accuracy, bottom

*Corresponding author: yongliz@outlook.com
[a]orcid.org/0009-0002-4201-3400
DOI: http://dx.doi.org/10.17515/resm2026-1886vk0716rs

heat duty, product purity, and thermal degradation risk under vacuum conditions. This feature requires the following focus on the logic of "polar close-boiling mixed phenols-vacuum distillation-dynamic stability" rather than on general distillation methods only. Because of the importance and complexity of phenol separation in coal tar, its efficient separation and refining has become a research hotspot in the modern coal chemical industry, and has economic and environmental significance. However, traditional solvent extraction and chemical washing suffer from high solvent consumption, substantial wastewater generation, and limited selectivity. Lv Q et al. conducted a comprehensive review of the extraction of phenols from coal tar. By deeply analyzing its component distribution and separation mechanism, exploring new green separation processes has become an inevitable trend to realize the high-value utilization of coal tar [6]. To overcome the pollution and energy consumption problems in traditional processes, Guo J et al. proposed an environmentally friendly conceptual design process. The process simultaneously and efficiently extracted phenols and naphthalene compounds in tar, significantly improving the overall separation efficiency of the system [7]. Yang Z X et al. used choline chloride-urea deep eutectic solvent to extract phenolic compounds from coal tar, and the experimental results showed that the method achieved effective separation of phenol and cresol components based on liquid-liquid phase equilibrium and hydrogen-bond interaction [8]. This provides a reference for understanding the phase behavior and separation characteristics of polar phenolic systems.

For coal tar mixed phenols with strong polarity and close-boiling characteristics, the property method directly affects column-sequence judgment, theoretical-stage number, reflux ratio, and heat-duty calculation. Therefore, the thermodynamic model is the starting point of the steady-state process design in this work. Fonseca F G et al. explored the Vapor-Liquid Equilibrium (VLE) of pyrolysis bio-oil (rich in phenols). The activity coefficient model such as Non-random Two-liquid (NRTL) had extremely high prediction accuracy when dealing with highly polar and non-ideal mixture systems [9]. For steady-state distillation architecture design, the separation sequence directly determines the energy consumption and equipment investment. Tang W T et al. compared various separation alternatives for industrial multi-component mixtures. By optimizing the complex column sequence and topology, the total annual cost of the entire process could be effectively reduced [10]. Although the pressure-swing heat-integrated distillation obtained by Yin et al. concerns an azeotropic system, its principles of pressure selection, heat integration, and parameter optimization provide design guidance for the four-columns vacuum process [11]. These process design theories provide some guidance for the continuous four-columns vacuum distillation separation of mixed phenols.

Steady-state optimization can only determine the column structure and operating parameters under nominal conditions. However, the composition of coal tar crude phenols is strongly affected by upstream feed fluctuations. Changes in feed flow rate or composition can propagate through the four columns and amplify the coupled fluctuations of column temperature, reflux flow, and product purity. Therefore, dynamic control is not an additional topic, but a necessary part to ensure the operability of continuous processes. As a typical multiple-input multiple-output (MIMO) system, a multi-component distillation column exhibits strong coupling and large time-delay characteristics. The development of its dynamic control strategy is the core of ensuring product quality. Flores-Gómez L R et al. evaluated fractional-order controllers in an extractive distillation column, and the results showed that the optimized controller improved the dynamic response and control stability of the column compared with conventional control strategies [12]. This provides a reference for the dynamic control design of strongly coupled distillation systems. For control under specific operating modes, Qu Q et al. constructed an optimal control framework for semi-continuous distillation. The system exhibited greater adaptive adjustment capabilities when dealing with feed fluctuations [13]. To improve the response speed and robustness of the control system, advanced control algorithms have been largely introduced into the field of distillation. Qian X et al. applied a model predictive control method based on dynamic mode decomposition. This algorithm more accurately predicted multi-variable complex dynamic behaviors and effectively shortened the adjustment time [14]. Guo et al. showed that feedforward-feedback cascade control using sensitive-tray temperature as the controlled variable can suppress product-quality deviations caused by feed disturbances [15].

In summary, many experts have explored the purification and steady-state separation processes of phenolic compounds in coal tar, as well as the thermodynamic modeling and dynamic control algorithms of complex distillation systems. Existing studies have addressed crude phenol separation processes, property methods, and distillation control, but these three aspects are often discussed separately. Steady-state process studies rarely further examine product-quality recovery under disturbances, while control studies are mostly based on general distillation systems and do not sufficiently consider the thermal sensitivity, close-boiling separation difficulty, and cumulative disturbance characteristics of series-connected mixed-phenol columns. Minor feed disturbances first alter the T101 bottoms stream and are then transmitted successively as the feed to downstream columns, accumulating material- and energy-balance deviations, amplifying T104 purity fluctuations, and prolonging recovery. Therefore, the study proposes a steady-state process design for continuous four-columns vacuum distillation of coal tar mixed phenol and a temperature-concentration cascade dynamic control strategy based on feedforward compensation. The research innovations are as follows: Based on the highly polar thermodynamic characteristics of the phenolic system, taking into account product purity and material thermal constraints, the continuous four-columns pressure reduction separation sequence is reconstructed and optimized from the steady-state level. Breaking the limitation of isolated steady-state investigations, a temperature-concentration cascade control system with feedforward compensation is developed based on the coupling characteristics of the four-columns process. A dynamic mathematical model is constructed to reveal the transient energy compensation mechanism, providing a feasible path for mixed phenol refining.

## 2. Design of Continuous Four-Columns Vacuum Distillation Process and Control Strategy

### 2.1 Raw Material Characteristics and Thermodynamic Physical Property Method Selection

The coal tar mixed phenol system has an extremely complex composition, mainly including phenol, o-cresol, m-cresol, p-cresol and xylenol and other homologues [16]. The boiling point differences between the components of this system are non-uniformly distributed, especially the boiling points of m-cresol and p-cresol are close, and their relative volatility is close to 1, which is a typical heat-sensitive system that is difficult to separate [17]. To accurately carry out process simulation and steady-state design, the feed composition of the mixed phenol raw materials and their basic thermodynamic parameters are first clarified. The specific parameters are detailed in Table 1.

Table 1. Feed composition and basic thermodynamic properties of coal tar mixed phenols

| Component | Mass Fraction (%) | Molar Flow Rate (kmol/h) | Normal Boiling Point (°C) | Critical Temperature (K) | Critical Pressure (bar) |
|---|---|---|---|---|---|
| Phenol | 35.2 | 45.1 | 181.7 | 694.2 | 61.3 |
| o-Cresol | 20.5 | 22.8 | 191 | 697.5 | 50.1 |
| m-Cresol | 25.1 | 27.9 | 202.3 | 705.8 | 45.6 |
| p-Cresol | 12.4 | 13.8 | 201.9 | 704.5 | 51.5 |
| Xylenols | 6.8 | 6.7 | 211–225 | 730 | 43.5 |

Table 1 represents the phenolic design feed after water settling, dewatering, and light-end removal, with the composition renormalized on an anhydrous phenolic basis. Before entering T101, the industrial feed should pass through an upstream dewatering and light-end removal unit, reducing water and light neutral oils to no more than 0.05 wt% and 0.10 wt%, respectively. The baseline feed rate was 116.3 kmol/h, corresponding to approximately 12.04 t/h. Before entering stage 28 of T101, the feed was preheated to 140 °C and maintained at 20 kPa. The flash calculation identified the feed as a saturated liquid. Both the liquid fraction and the feed thermal-state parameter used in the Underwood calculation were therefore set to 1.00. Critical properties and normal boiling points were retrieved from the Aspen Physical Property System used in this study. Xylenols were treated as a lumped isomeric pseudo component. Therefore, their boiling point is reported as a

range. After determining the basic properties of the raw materials, the rational selection of thermodynamic property methods is the core link to ensure the simulation accuracy of the vacuum distillation process. Since the coal tar mixed phenol system contains a large number of polar molecules and exhibits extremely significant non-ideal vapor-liquid equilibrium characteristics under negative pressure conditions, conventional equations of state cannot accurately describe its phase behavior. Therefore, this study uses a NRTL activity coefficient model to calculate the liquid phase non-ideality of the multi-component system. This model can accurately characterize the complex interactions between polar compounds. To ensure the traceability and reproducibility of property calculations, steady-state simulations are performed using the rigorous RadFrac module in Aspen Plus with the NRTL-HOC property method. NRTL describes liquid-phase non-ideality, whereas HOC corrects vapour-phase association. Binary interaction parameters are preferentially taken from the Aspen Plus database. Missing or incomplete parameters are regressed against literature VLE data. The activity coefficients required for simultaneous solution in this physical process are shown in Equation (1).

$$\begin{cases} ln\,\gamma_i = \dfrac{\sum_j x_j\,\tau_{ji} G_{ji}}{\sum_j x_j\,G_{ji}} + \sum_j \dfrac{x_j G_{ij}}{\sum_k x_k\,G_{kj}}\left(\tau_{ij} - \dfrac{\sum_k x_k\,\tau_{kj} G_{kj}}{\sum_k x_k\,G_{kj}}\right) \\ \tau_{ij} = a_{ij} + \dfrac{b_{ij}}{T}, \quad G_{ij} = exp(-\alpha_{ij}\tau_{ij}), \quad \alpha_{ij} = \alpha_{ji} = 0.30 \end{cases} \tag{1}$$

In Equation (1), $\gamma_i$ represents the activity coefficient of the component $i$ in the solution. $x_j$, $x_k$, and $x_m$ represent the mole fractions of components $j$, $k$, and $m$ in the liquid phase, respectively. $T$ is the absolute temperature of the system, measured by Kelvin. $n$ represents the total number of components in the system. $\tau_{ji}$ and $\tau_{ij}$ are dimensionless interaction energy parameters between components. $G_{ji}$ and $G_{ij}$ are local composition parameters related to non-randomness. $\alpha_{ji}$ is a non-randomness parameter characterizing the non-randomness of the mixture and satisfies the constant symmetry condition. $a_{ji}$ and $b_{ji}$ are the fitting constants for the temperature dependence of the binary interaction parameters. The parameter form is defined as $\tau_{ij} = a_{ij} + b_{ij}/T$, and the non-randomness parameter is uniformly set as $a_{ij}$=0.30. The non-randomness parameter is initialized at 0.30 and jointly regressed with the temperature-dependent binary interaction parameters against literature VLE data by minimizing deviations in vapor-phase composition and equilibrium temperature. The value of 0.30 is retained only when freeing this parameter produced no significant improvement. The final Aspen Plus input is checked: the non-randomness field is set to 0.30 for every binary pair, and the first value listed for each pair is entered in the forward temperature-independent binary interaction-parameter field represented by the lowercase Latin letter a. The main binary parameters used in the simulation are as follows: for phenol-o-cresol, $a_{ij}$=0.214, $b_{ij}$=-86.5, $a_{ji}$=-0.137, and $b_{ji}$=128.4. For phenol-m-cresol, $a_{ij}$=0.236, $b_{ij}$=-92.8, $a_{ji}$=-0.151, and $b_{ji}$=137.6. For phenol-p-cresol, $a_{ij}$=0.228, $b_{ij}$=-89.3, $a_{ji}$=-0.146, and $b_{ji}$=132.1. For phenol-xylenols, $a_{ij}$=0.318, $b_{ij}$=-121.7, $a_{ji}$=-0.204, and $b_{ji}$=168.9. For o-cresol-m-cresol, $a_{ij}$=0.082, $b_{ij}$=-34.6, $a_{ji}$=-0.061, and $b_{ji}$=42.3. For o-cresol-p-cresol, $a_{ij}$=0.076, $b_{ij}$=-31.8, $a_{ji}$=-0.054, and $b_{ji}$=39.7. For m-cresol-p-cresol, $a_{ij}$=0.028, $b_{ij}$=-12.5, $a_{ji}$=-0.021, and $b_{ji}$=15.4. For cresol isomers-xylenols, $a_{ij}$ ranges from 0.115 to 0.156, $b_{ij}$ ranges from -52.4 to -68.7, $a_{ji}$ ranges from -0.083 to -0.112, and $b_{ji}$ ranges from 63.5 to 84.2. These parameters are used to describe the liquid-phase non-ideality among phenol, cresol isomers, and xylenols, and served as the unified thermodynamic basis for the subsequent calculations of theoretical stages, reflux ratio, heat duty, and dynamic control. The activity coefficients calculated by the above simultaneous equations can provide extremely reliable thermodynamic data support for the subsequent global material balance and energy balance calculations of the continuous four-columns vacuum distillation process.

### 2.2 Architecture and Parameter Design of Steady-State Four-Columns Vacuum Distillation Process

After establishing thermodynamic property methods, a global architecture for steady-state four-columns vacuum distillation is constructed to achieve high-purity extraction of phenol, o-cresol,

m/p-cresol, and xylenol. This process employs a direct separation sequence, with the material flowing sequentially through four vacuum distillation columns. This arrangement effectively reduces the heat load at the bottom of each column according to the increasing boiling point of the components, thereby protecting the heat-sensitive phenolic components, as shown in Figure 1.

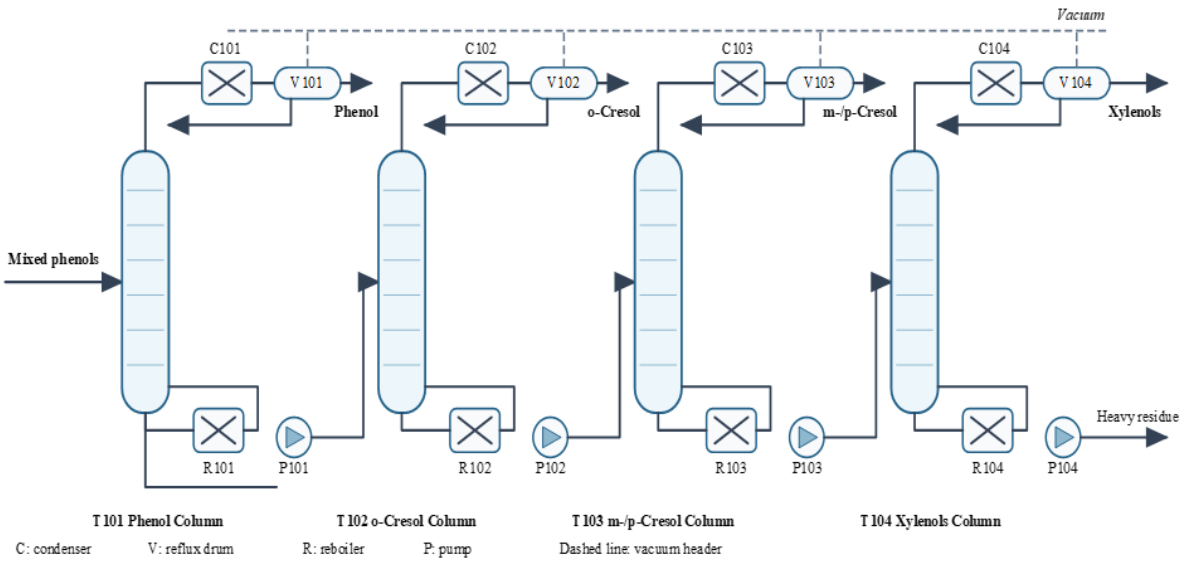


Fig. 1. Flow chart of continuous four-columns vacuum distillation process for coal tar mixed phenols

Figure 1 presents the continuous four-columns vacuum distillation process of coal tar mixed phenol (PFD). The diagram details how the material is separated in cascades between the phenol column (T101), o-cresol column (T102), m/p-cresol column (T103), and xylenol column (T104) after the feed is fed. The condensers, reflux drums, reboilers, and pumps of T101-T104 are consistently labelled, and the T104 overhead product stream is identified as xylenols. The T103 column is not designed to separate m-cresol and p-cresol into individual high-purity products, but to obtain an m-/p-cresol mixed fraction. Because the boiling points of m-cresol and p-cresol are close and their relative volatility is close to unity, their economical separation by conventional vacuum distillation is difficult. Therefore, the product purity of T103 is defined as the total mass fraction of m-cresol and p-cresol in the mixed fraction, namely w(m-cresol+p-cresol), rather than the individual purity of m-cresol and p-cresol both exceeding 99%. If high-purity single m-cresol or p-cresol products are required, additional separation methods such as crystallization, extraction, adsorption, or other specialized processes should be introduced, which is beyond the present four-columns vacuum distillation process. The four-columns steady-state flowsheet is established under unified boundary conditions. The feed composition is taken from Table 1, and the operating pressure is set at 18.0 kPa with internal column pressure drop considered. A total condenser and a kettle reboiler are used for each column. Because the freezing points of high-purity phenol and o-cresol are 40.8 °C and 30.9 °C, respectively, the T101 and T102 overhead condensers use a closed hot-water loop operated at 50-60 °C. Heat tracing and low-temperature alarms and interlocks are provided to keep the heat-transfer surfaces and reflux lines above the corresponding freezing points. Circulating cooling water is used for T103 and T104 after solidification-risk screening. The number of stages, feed location, and reflux ratio are first estimated using the Fenske-Underwood method and then iteratively optimized in the RadFrac module with product purity, recovery and heat duty as the target indicators. To determine the optimal structural parameters of the distillation column, the preliminary values of the theoretical plate number and reflux ratio are obtained by a simple calculation method. The minimum theoretical plate number is estimated by the Fenske equation, as shown in Equation (2) [18].

$$N_{min} = \frac{ln[(\frac{x_L}{x_H})_D(\frac{x_H}{x_L})_B]}{ln\,\alpha_{avg}} \tag{2}$$

In Equation (2), $N_{min}$ represents the minimum number of theoretical plates required for distillation to achieve the specified separation requirements. $x_L$ and $x_H$ represent the mole fractions of the light key component and the heavy key component in the overhead distillate $D$ and bottom residue $B$, respectively. $\alpha_{avg}$ represents the average relative volatility of the system under the average operating pressure. Meanwhile, the minimum reflux ratio depends on the Underwood equation, as shown in Equation (3).

$$1 - q = \sum_{i=1}^{n} \frac{\alpha_i x_{Fi}}{\alpha_i - \theta} \tag{3}$$

In Equation (3), $q$ is a parameter characterizing the thermal state of the feed. The value used in the shortcut calculation was 1.00, corresponding to the saturated-liquid feed specified in Section 2.1. $\alpha_i$ is the relative volatility of the component $i$ relative to the reference component. $x_{Fi}$ is the mole fraction of the component $i$ in the feed liquid. $\theta$ is the root of the equation, whose value is usually limited to the relative volatility values of the two key components. $n$ is the total number of components involved in the calculation. After the Underwood root is obtained from Equation (3), the minimum reflux ratio is determined by dividing, for each distillate component, the product of relative volatility and distillate mole fraction by the difference between relative volatility and the root, summing the resulting terms, and subtracting unity. The minimum theoretical stages for T101-T104 are 32, 37, 42, and 26, and the corresponding minimum reflux ratios are 2.13, 2.73, 3.67, and 1.87. The RadFrac-optimised stage numbers and reflux ratios are 55/3.2, 62/4.1, 70/5.5, and 45/2.8, respectively. After calculating macroscopic parameters, the physical design of the column internals needs to take into account both the requirements of low pressure drop and high efficiency. All four columns use Mellapak 250Y structured packing to minimize pressure drop and high-temperature residence time under vacuum. An HETP of 0.45 m is used only to convert the optimized equilibrium-stage counts into preliminary packed heights. The RadFrac separation calculation remains stage-based. Allowances for liquid distributors and installation are added separately during engineering sizing.

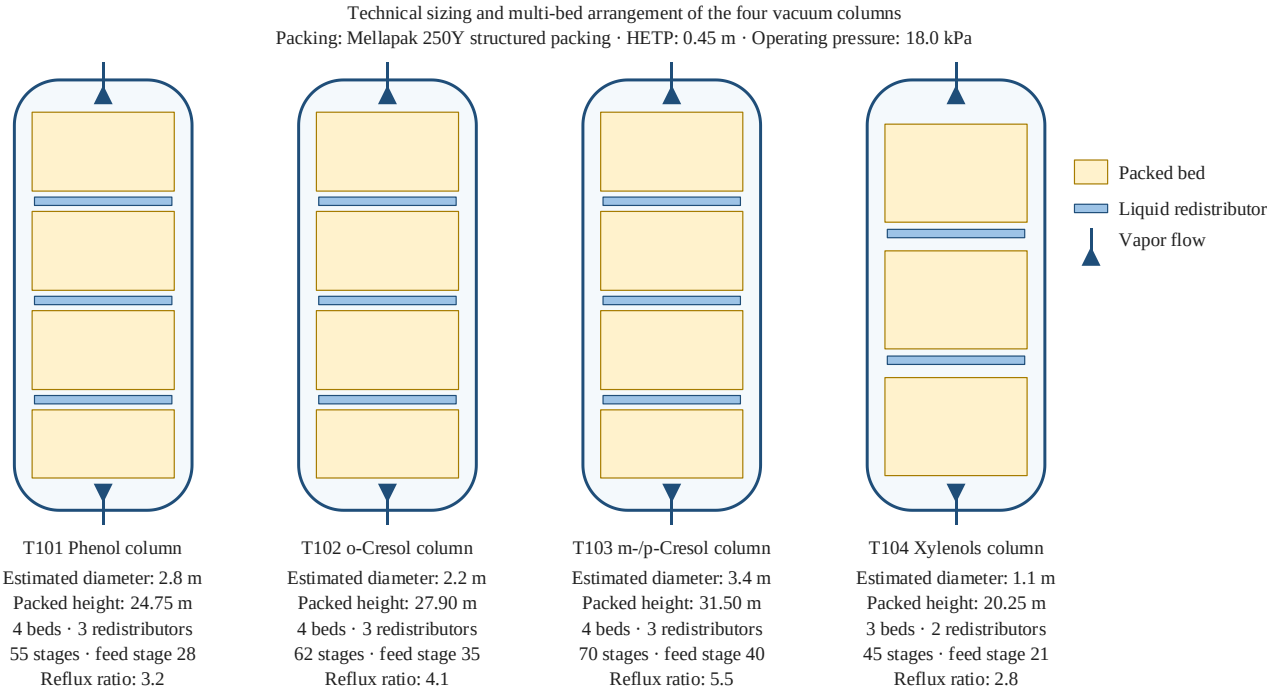


Fig. 2. Process-specific sizing and multi-bed hydraulic arrangement of columns T101-T104

Figure 2 presents the preliminary engineering dimensions and multi-bed arrangements of the four columns. T101-T104 employ Mellapak 250Y structured packing, with preliminary diameters of 2.8, 2.2, 3.4, and 1.1 m and packed heights of 24.75, 27.90, 31.50, and 20.25 m, respectively. The first

three columns contain four packed beds and three intermediate liquid redistributors, whereas T104 contains three beds and two redistributors. The diameters are preliminarily estimated from vapor loads at 18.0 kPa using approximately 80% of flooding capacity and should be confirmed by Aspen hydraulic rating.

### 2.3 Mathematical Model and Tuning Algorithm of Dynamic Control Strategy

Establishing a dynamic mathematical model for multi-component vacuum distillation is the basis for designing control strategies. Its core lies in accurately describing the mass and energy conservation process within each equivalent theoretical stage of the packed beds. The dynamic model is established by importing the converged Aspen Plus steady-state flowsheet into Aspen Dynamics, while retaining the state variables of sump holdup, reflux-drum holdup, pressure, temperature, and composition. The control structure includes pressure control, level control, sensitive-tray temperature control, and product-composition soft-sensor control. The composition feedback is not assumed to be an ideal instantaneous concentration signal, but is estimated from sensitive-tray temperature, column pressure, reflux flow rate, feed flow rate, and reboiler duty. A pressure-driven rigorous unsteady-state column model is adopted rather than applying empirical disturbances to steady-state results only. Dynamic holdups in the condenser, reflux drum, reboiler, and column liquid phase are retained for all four columns. The reboiler holdups of T101-T104 are set as 8.5, 7.8, 9.2, and 6.5 kmol, respectively, while the reflux drum holdups are set as 3.0, 2.8, 3.5, and 2.4 kmol. The liquid holdups are determined from the product of the nominal liquid flow rate and residence time. For T101-T104, the nominal reboiler liquid flow rates are 85, 78, 92, and 65 kmol·h-1 with a 6 min residence time. The reflux-drum values are 36.0, 33.6, 42.0, and 28.8 kmol·h-1 with a 5 min residence time. The packed beds were discretized into equivalent theoretical stages using an HETP of 0.45 m. A first-order liquid-hydraulic lag was adopted in Aspen Dynamics, with a nominal lag time of 2.0 min for each packed bed, while the dynamic liquid holdup varied with the 0.50 power of the liquid load. Based on this model, a ±20% change in holdup altered the settling time of T101 from 45 min to 43-47 min and the maximum purity deviation from 0.08% to 0.07%-0.09%. The liquid-level set point is fixed at 50% of the effective equipment volume. The top pressure of each column is set at 18.0 kPa, with an allowable fluctuation range of ±0.5 kPa, and is regulated jointly by condenser duty and the vacuum system. Sensitive trays are selected according to the maximum steady-state temperature-composition sensitivity while avoiding the feed stage. Therefore, stages 34, 42, 48, and 30 are selected as the temperature-control trays for T101-T104, respectively. When ignoring the amount of gas phase retention and assuming complete mixing of the liquid phase, the total mass conservation differential equation of the $j$ -layer tray is shown in Equation (4) [19].

$$\frac{dM_j}{dt} = L_{j-1} + V_{j+1} + F_j - L_j - V_j \tag{4}$$

In Equation (4), $M_j$ represents the liquid phase molar retention on the $j$ -th tray. $t$ represents the independent variable time of the dynamic response. $L_{j-1}$ represents the molar flow rate of the liquid phase flowing from the upper layer, that is, the $j-1$-th tray. $V_{j+1}$ represents the molar flow rate of the gas phase rising from the next layer, the $j+1$-th tray. $F_j$ is the feed molar flow rate of the tray. $L_j$ and $V_j$ respectively represent the molar flow rates of the liquid phase and gas phase flowing out of the tray. Based on the overall mass conservation, the component mass conservation equation for a specific component $i$ in the system needs to be further calculated, as shown in Equation (5) [20].

$$\frac{d(M_j x_{i,j})}{dt} = L_{j-1}x_{i,j-1} + V_{j+1}y_{i,j+1} + F_j z_{i,j} - L_j x_{i,j} - V_j y_{i,j} \tag{5}$$

In Equation (5), $x_{i,j}$ and $x_{i,j-1}$ represent the mole fractions of the component $i$ in the liquid phase of the $j$ and $j-1$ trays, respectively. $y_{i,j+1}$ and $y_{i,j}$ represent the mole fractions of the component $i$ in the gas phase of the $j+1$ and $j$ trays, respectively. $z_{i,j}$ is the mole fraction of the component $i$ in the feed. Based on the above rigorous mechanistic model, a global dynamic architecture

including a basic loop of liquid level and pressure and a higher-order regulation loop is constructed, as shown in Figure 3.

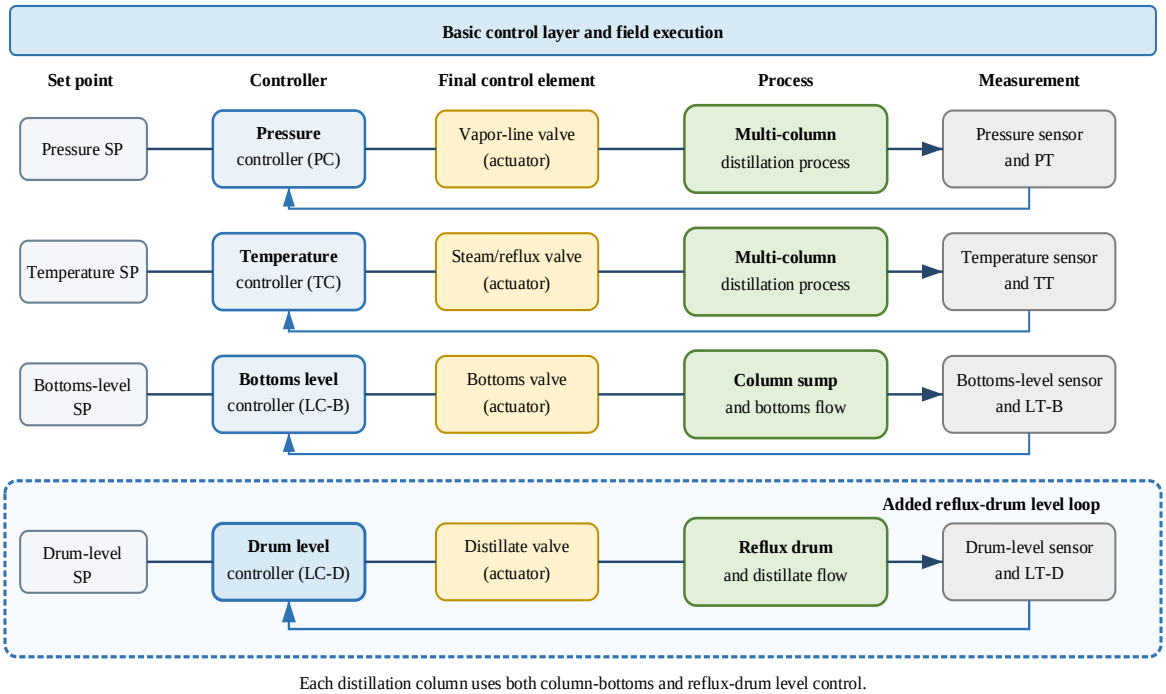


Fig. 3. Architecture and signal transmission of the global dynamic control system for multi-column distillation

Figure 3 illustrates the overall topology from the basic control loops for liquid level and pressure to the temperature control loop, using a standard system architecture logic block diagram. It clearly shows the closed-loop logic relationship between sensor measurement, transmitter signal transmission, and actuator valve opening adjustment. Because the vacuum distillation process exhibits strong nonlinearity and large hysteresis, single temperature control is insufficient to guarantee product purity during feed fluctuations. Therefore, a temperature-concentration cascade control algorithm with feedforward compensation is developed, as shown in Equation (6).

$$u(t) = u_0 + K_c\left[e(t) + \frac{1}{T_i}\int_0^t e(\tau)d\tau + T_d\frac{de(t)}{dt}\right] \tag{6}$$

In Equation (6), $u(t)$ is the adjustment signal output by the controller to the actuator at time $t$. $K_c$ is the proportional gain constant of the controller, which determines the initial strength of the system's response to error. $e(t)$ represents the real-time deviation between the set value and the actual measured value. $T_i$ is the integral time constant, used to eliminate the steady-state residual of the system. $\tau$ is the time integration variable in the integral operation process. $T_d$ is the derivative time constant, used to provide advance adjustment based on the rate of change of deviation. The controller bias is the nominal valve position at zero error. The feedforward path superposes feed-flow and key-component mass-fraction disturbances. Each branch uses the negative ratio of the disturbance-path model to the manipulated-path model, implemented as a lead-lag element. The total command is the sum of the bias, PID feedback, and feedforward compensation and remains subject to the stated valve-position, rate, and dead-band constraints, as shown in Equation (7).

$$\begin{cases} \Delta u_{ff}(s) = G_{ff,F}(s)\Delta F(s) + G_{ff,z}(s)\Delta z(s) \\ G_{ff,j}(s) = -\dfrac{G_{d,j}(s)}{G_u(s)} = K_{ff,j}\dfrac{(\tau_{lead,j}s+1)}{(\tau_{lag,j}s+1)}, j \in \{F,z\} \end{cases} \tag{7}$$

In the actual tuning process, the initial value is obtained by the relay feedback method and the Tyreus-Luyben tuning rule. The optimal anti-disturbance performance is achieved through dynamic optimization, as shown in Figure 4.

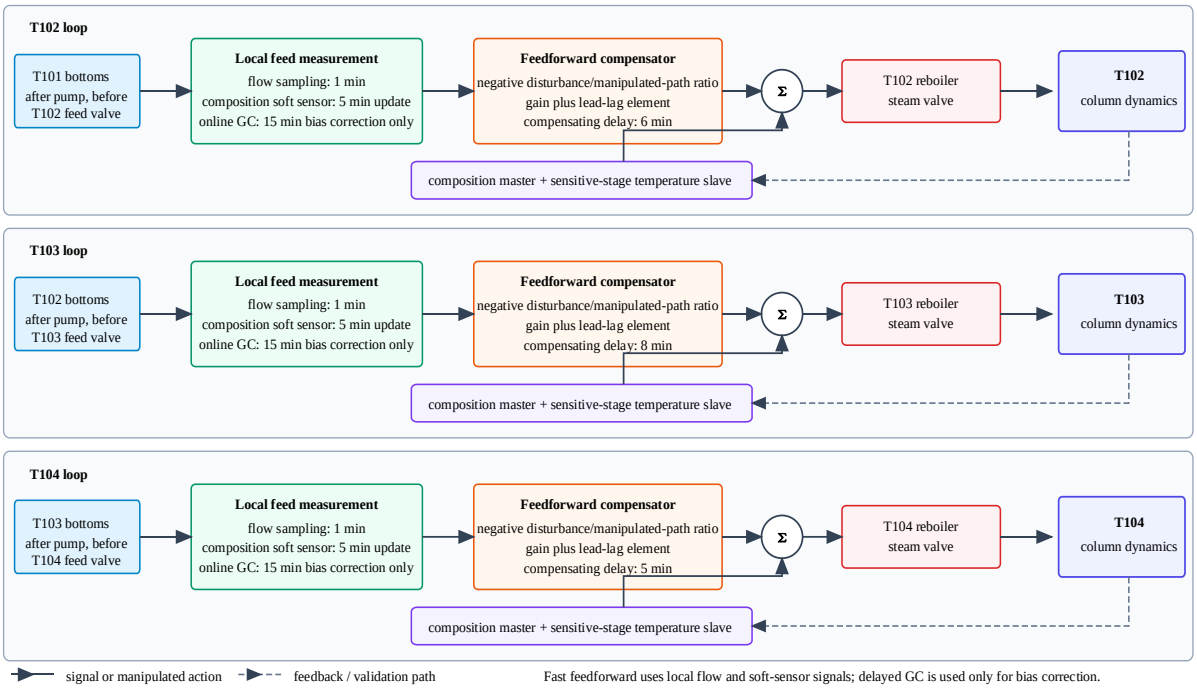


Fig. 4. Feedforward-feedback temperature-concentration cascade control strategy logic

Figure 4 is the algorithm control logic flow chart. It demonstrates in detail the logical judgment conditions and action execution steps of the main controller, that is, the concentration controller, and the secondary controller, that is, the sensitive plate temperature controller, to collaboratively calculate and adjust the heat load of the reboiler when the feed flow or concentration is disturbed. To avoid simplifying composition control as ideal concentration feedback, a soft-sensor-based concentration feedback scheme is adopted in the dynamic control system. The top or bottom product composition is not assumed to be directly and instantaneously measurable. Instead, it is estimated from online variables, including sensitive-tray temperature, column pressure, reflux flow rate, feed flow rate, and reboiler duty, combined with the NRTL thermodynamic model and dynamic material balance. Online gas chromatography can be used for steady-state validation and parameter correction, but it is not taken as the only input for fast closed-loop control. The concentration controller corrects the sensitive-tray temperature set point according to the estimated composition deviation, and the secondary temperature loop further adjusts the reboiler steam valve opening. The feedforward path pre-corrects the heat duty according to feed flow and composition disturbances, thereby reducing the influence of composition-analysis delay on control performance. The dynamic simulation is established by importing the steady-state Aspen Plus model into Aspen Dynamics, and the model file, control modules, and disturbance scripts are provided as Supplementary File S1. The sensitive tray is selected according to the maximum steady-state temperature-composition sensitivity of each column while avoiding the feed tray, namely the tray with the peak value of $|\partial xD/B/\partial Tj|$. The sampling periods of temperature, pressure, and liquid level are set to 1.0, 0.5, and 1.0 min, respectively. The composition soft sensor is updated every 5 min, with a 15 min delay assigned to online chromatographic correction. Equal-percentage steam and reflux valves are used as actuators, with an opening range of 0-100%, a maximum rate of change of 10%·min-1, and a dead band of 1%. The primary controlled variable is the soft-sensed product composition, the secondary controlled variable is the sensitive-tray temperature, and the manipulated variables are reboiler duty and reflux flow rate. The feedforward path pre-compensates the reboiler duty according to changes in feed flow rate and key-component mass fraction. The feedforward signals for T102, T103, and T104 are obtained from the flow rate and soft-sensed key-component fraction of the T101, T102, and T103 bottoms streams, respectively,

measured downstream of the bottoms pump and upstream of the downstream-column feed valve. The fresh-feed signal of T101 is not used directly. Consistent with Equation (7), gain and lead-lag compensation are applied, with initial compensating delays of 6, 8, and 5 min, respectively. Flow signals are updated every 1 min and soft-sensor estimates every 5 min. The online GC delay of 15 min is used only for bias correction and is excluded from the fast feedforward loop.

## 3. Results and Discussion

### 3.1 Steady-State Design Calculation Results and Overall Column Distribution Characteristics of The Four-Columns Process

Based on the aforementioned rigorous thermodynamic model and process architecture design, the global steady-state calculation of the continuous four-columns vacuum distillation process was completed in chemical simulation platforms such as Aspen Plus, and the high-purity separation of each phenolic component was successfully achieved. Table 2 summarizes in detail the core data of the steady-state process optimization parameters and energy consumption distribution of the four-columns vacuum continuous distillation.

Table 2. Optimization parameters and energy consumption distribution of steady-state process for continuous four-columns vacuum distillation

| Column ID | Theoretical Stages | Feed Stage | Reflux Ratio | Top Pressure (kPa) | Top/Bottom Temperature (°C) | Condenser Duty (kW) | Reboiler Duty (kW) | Product Purity (wt%) | Recovery (%) |
|---|---|---|---|---|---|---|---|---|---|
| T101 (Phenol) | 55 | 28 | 3.2 | 18 | 112.5/142.0 | 1420.5 | 1580.2 | 99.8 | 99.1 |
| T102 (o-Cresol) | 62 | 35 | 4.1 | 18 | 132.4/158.5 | 1150.8 | 1295.4 | 99.5 | 98.7 |
| T103 (m-/p-Cresol) | 70 | 40 | 5.5 | 18 | 148.6/175.0 | 1680.3 | 1850.6 | 99.2[a] | 98.2 |
| T104 (Xylenol) | 45 | 21 | 2.8 | 18 | 165.2/192.1 | 890.1 | 960.5 | 99 | 97.5 |

Table 2 lists the optimized process parameters and energy consumption distribution of the four continuous vacuum distillation columns (T101, T102, T103, and T104) under steady-state conditions. T103 has 70 theoretical stages, a reflux ratio of 5.5, a condenser duty of 1680.3 kW, and a reboiler duty of 1850.6 kW, all of which are the highest among the four columns. T104 has 45 theoretical stages, a reflux ratio of 2.8, a condenser duty of 890.1 kW, and a reboiler duty of 960.5 kW. Product purity is at least 99% for all columns, with T101 reaching 99.8%, while recovery is at least 97.5%, with T101 reaching 99.1%. The feed-stage location and total number of theoretical stages were coordinated for each column to ensure effective separation and reasonable energy consumption. Feed-temperature sensitivity was estimated at 20 kPa. At 130 °C, the feed became slightly subcooled, the thermal-state parameter increased to approximately 1.05, and the T101 reboiler duty increased to 1654 kW. At 150 °C, the parameter decreased to approximately 0.95 and the duty decreased to 1507 kW. Both deviations were approximately 4.7% relative to the baseline duty of 1580.2 kW. To further reveal the thermodynamic and mass transfer microstates within each column under optimal conditions, Figure 5 illustrates the temperature, concentration, and phase distribution characteristics of the entire column during steady-state operation.

Figure 5(a) shows the temperature distribution across the entire column, with the top and bottom temperatures of T101 to T104 exhibiting a gradient increase from 112.5 to 142.0°C, 132.4 to 158.5°C, 148.6 to 175.0°C, and 165.2 to 192.1°C, respectively. The maximum temperature changes in T101, T102, T103, and T104 occur at relative stage positions of 0.51, 0.56, 0.57, and 0.47, respectively, consistent with the actual feed stages in Table 2. Figure 5(b) presents continuous liquid-phase mole-fraction profiles of phenol, o-cresol, m-cresol, p-cresol, and xylenols over all

theoretical stages of T101. Stage efficiency is calculated as the ratio of the actual key-component composition change in the outgoing vapor to the change required for vapor-liquid equilibrium and is then averaged using vapor load as the weighting basis. Low-load operation tends toward weeping, whereas high-load operation tends toward entrainment and flooding, reducing the efficiency from 72.8% to a minimum of 45.2%.

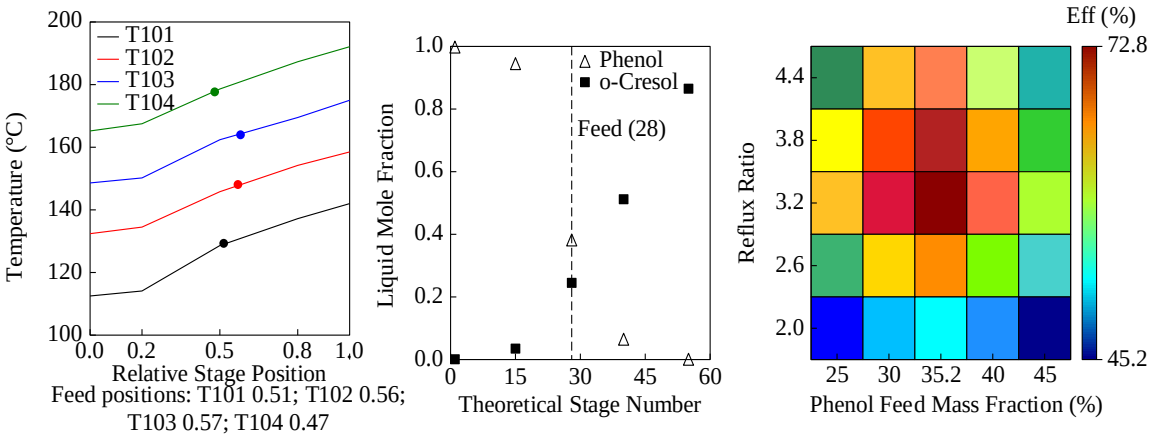


(a) Temperature profiles and actual relative feed-stage positions

(b) Concentration distribution scatter plot

(c) Tray separation efficiency

Fig. 5. Changes in temperature, concentration, and phase distribution during steady-state operation

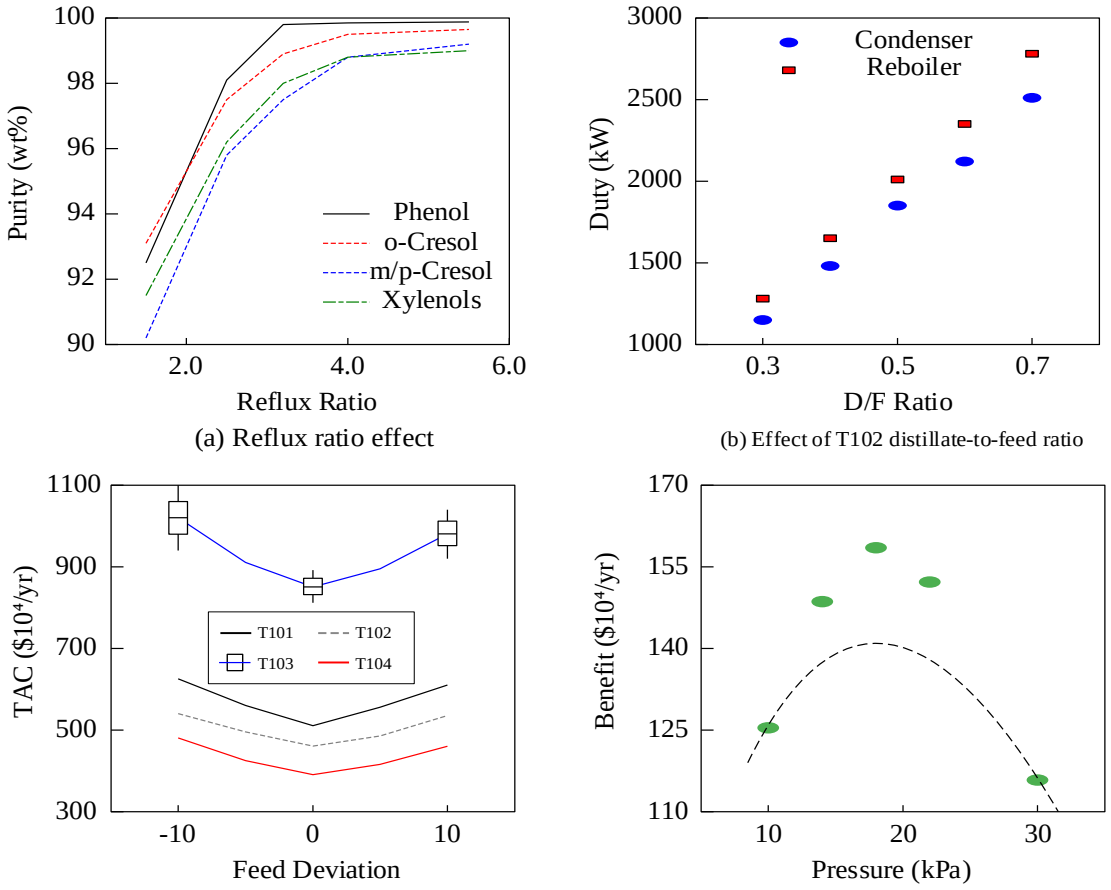


(a) Reflux ratio effect

(b) Effect of T102 distillate-to-feed ratio

(c) Feed plate position offset

(d) Operating pressure

Fig. 6. Comprehensive impact of process operating parameters on product purity and heat load

The comprehensive separation efficiency reaches a maximum of 72.8%. For each stage, the efficiency is calculated as the ratio of the actual change in the key-component composition of the outgoing vapor to the change required to reach vapor-liquid equilibrium, and the column-average value is obtained by weighting the stage values by vapor load rather than imposing a constant input.

Away from the nominal condition, low-load operation tends toward weeping, whereas high-load operation tends toward entrainment and flooding, reducing effective vapor-liquid contact and lowering the efficiency to 45.2%. Figure 6 presents the comprehensive impact of process operating parameters on product purity and heat load.

Figure 6(a) presents the effect of reflux ratio. When the reflux ratio increased from 1.5 to 4.0, the purity of phenol and m/p-cresol increased from 92.50% and 90.20%, and eventually stabilized at nonlinear limit thresholds of 99.85% and 98.80%. Based on T102, Figure 6(b) shows the effect of the distillate-to-feed ratio on heat duties. As this ratio increased from 0.3 to 0.7, the reboiler duty increased from 1280.5 to 2780.2 kW. To avoid presenting the economic evaluation only as numerical results, the total annual cost and comprehensive economic benefit were calculated under unified boundary conditions. The equipment investment included four distillation columns, condensers, reboilers, vacuum systems, reflux pumps, and auxiliary instruments, and was estimated from the simulated column diameter, column height, heat-transfer area, and vacuum load using conventional chemical equipment cost correlations. With hot-water supply and return temperatures of 50 and 60 °C, the circulation rates for T101 and T102 were estimated as 122.3 and 99.1 t/h, respectively. Assuming an overall heat-transfer coefficient of 0.60 kW/($m^2$·K) and a 15% area allowance, the preliminary condenser areas were estimated as 47.5 and 28.5 m2, respectively. The annualization factor was calculated with a depreciation period of 10 years and an annual interest rate of 8%. The operating cost included heating steam, hot-water circulation for T101 and T102, indirect cooling water, circulation pumping, electricity, and vacuum maintenance. Based on a loop pressure drop of 200 kPa, a pump efficiency of 70%, and a makeup rate of 1%, the annual hot-water-system operating cost was estimated as USD 0.1323 million, representing an increase of USD 0.0437 million per year over the direct-cooling-water case. Product revenue was calculated from the flow rate, purity, and average market price of phenol, o-cresol, m-/p-cresol mixed fraction, and xylenol products, while the raw-material cost was deducted according to the mixed-phenol feed rate. The total annual cost was calculated as “annualized equipment investment + annual operating cost”, and the comprehensive economic benefit was calculated as “annual product sales revenue - raw-material cost - annual operating cost - annualized equipment investment”. Therefore, the values of USD 8.505 million, USD 10.204 million, and USD 1.585 million/year in Figures 6(c) and 6(d) were obtained from the above unified economic boundary conditions rather than directly inferred from heat duty alone. Figure 6(c) presents the feed plate position offset line and box plot. The solid black, dashed gray, and solid red curves represent T101, T102, and T104, respectively, whereas the box plot represents T103. A deviation of ±10% from the optimal position caused the annual total cost of column T103 to increase from the baseline of US$8.505 million to US$10.204 million. The cost variance and investment risk were greatest in this deep offset range. Figure 6(d) shows the sensitivity of the annual net economic margin to operating pressure. The economic margin was defined as the product sales revenue minus raw-material cost and the total annual cost of T101-T104, rather than the TAC of a single column. The maximum annual net economic margin was US$1.585 million/year at 18.0 kPa. This value corresponds to the original direct-cooling-water baseline; after including the additional hot-water-system cost, the corrected maximum annual net economic margin was approximately USD 1.541 million per year. Although the TAC of T103 alone reached US$8.505 million/year under the optimal feed-stage condition, the positive margin was obtained only after the sales revenue of phenol, o-cresol, m-/p-cresol mixed fraction, and xylenols was included. Therefore, Figure 6(c) reflects the cost sensitivity of T103, whereas Figure 6(d) reflects the net economic margin of the whole four-columns process. The product purity, recovery, and heat duty in Table 2 were obtained from the unified property model and rigorous RadFrac calculation described above. To verify the stability of the results, local perturbation calculations were performed for reflux ratio, feed stage, and operating pressure. When the key parameters changed slightly around their optimal values, the variation trends of product purity and heat duty were consistent with the results shown in Figures 5 and 6, indicating that the data in Table 2 were not single-point empirical estimates.

### 3.2 Dynamic Anti-Interference Response Analysis Under Feed Flow Disturbance

After completing the overall steady-state baseline design, the robustness of the control system to external operating condition fluctuations is verified. This study sets a step disturbance of ±10% to

examine the designed temperature-concentration cascade control system's ability to reconstruct the system's dynamic equilibrium. Table 3 details the PID tuning parameters of each control loop after optimization in dynamic simulation and provides key quantitative evaluation indicators for measuring disturbance rejection performance, including settling time and maximum dynamic deviation. The total dynamic simulation time was set as 120 min, the disturbance was introduced at 10 min, and the integration step was 0.05 min. The settling time was defined as the time required for product purity to return to and remain within ±0.15% of the set point. The maximum deviation was defined as the maximum absolute deviation of product purity from the steady-state set point after disturbance. The dynamic disturbance test used the optimal steady-state condition as the initial state. A ±10% step disturbance in feed flow rate and a ±5% disturbance in key component composition were introduced. The settling time was defined as the time required for product purity to return to and remain within ±0.15% of the set value, while the maximum deviation was defined as the maximum absolute deviation of product purity from the steady-state set value after disturbance. The IAE values in Table 3 were calculated from the absolute deviation of the primary-loop product mass fraction from its set point, rather than from the sensitive-stage temperature error. Integration covered 0-120 min, with the disturbance introduced at 10 min and zero error before the disturbance. The absolute deviations were accumulated using a 0.05 min integration step. Therefore, the IAE unit is wt%·min. Values of 1.25, 1.84, 2.10, and 0.95 represent the accumulated product-purity deviations over the complete response period.

Table 3. Dynamic controller tuning parameters and performance evaluation indicators

| Control Loop | Controller Role | Controller Gain (Kc) | Integral Time (Ti, min) | Derivative Time (Td, min) | Settling Time (min) | Max Deviation (%) | IAE Index |
|---|---|---|---|---|---|---|---|
| T101 Distillate Purity | Master (Purity) | 12.5 | 8.2 | 0.6[b] | 45 | 0.08 | 1.25 |
| T102 Distillate Purity | Master (Purity) | 15.8 | 10.5 | 0.8[b] | 52 | 0.12 | 1.84 |
| T103 Distillate Purity | Master (Purity) | 18.2 | 12 | 0.9[b] | 65 | 0.15 | 2.1 |
| T104 Distillate Purity | Master (Purity) | 10.4 | 7.5 | 0.5[b] | 40 | 0.09 | 0.95 |

Table 3 lists the tuning parameters and performance evaluation indicators of the dynamic controllers, covering four control loops. The listed parameters correspond to the primary product-purity controllers. The secondary controllers regulate the sensitive-stage temperatures at stages 34, 42, 48, and 30 of T101-T104, respectively. [b]Derivative times were preliminarily inferred from the stated Tyreus-Luyben tuning rule and should be verified against the actual Aspen Dynamics controller settings. The T103 controller had the highest gain (18.2), integral time (12 min), settling time (65 min), maximum deviation (0.15%), and IAE index (2.1). The T104 controller had the best performance (10.4), integral time (7.5 min), settling time (40 min), and IAE index (0.95), with a maximum deviation of 0.09%. The dynamic response characteristics of the system under a +10% step disturbance in feed flow rate are shown in Figure 7.

Figure 7(a) shows the purity response line graph. After the disturbance occurred at the 10th minute, the purity of m/p-cresol showed the maximum absolute deviation of 0.15% and dropped to 99.05%. Following controller action, the purities of the four products steadily returned to their respective set points within 40-65 min after the disturbance. Figure 7(b) presents sensitive-stage temperature deviations from their respective set points. T103 exhibited the largest increase of 1.7 °C. feedforward compensation limited the response to fewer than two oscillations and restored steady state by 70 min.

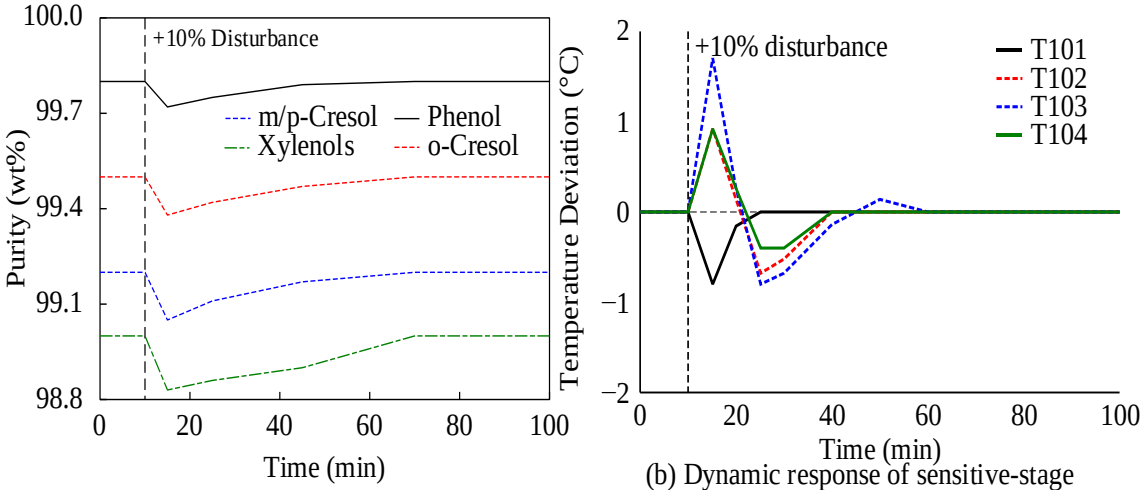


(a) Dynamic Response of Product Purity

(b) Dynamic response of sensitive-stage temperature deviation

Fig. 7. Dynamic response characteristics of the system under feed flow +10% step disturbance

### 3.3 Dynamic Adaptive Adjustment Analysis Under Changes in Feed Composition

In actual chemical production operations, fluctuations in upstream processes often lead to significant transient or steady-state abrupt changes in the feed composition of distillation columns. This places high demands on the dynamic maintenance of system energy balance and the baseline assurance of product purity. When the content of light or heavy components in mixed phenol feed undergoes a large abrupt change, the original vapor-liquid phase equilibrium and concentration gradient within the column are rapidly disrupted. The study specifically introduced harsh working conditions in which the content of key components such as phenol suddenly changes by ±5% in the dynamic simulation to deeply examine the dynamic compensation mechanism and adaptive adjustment performance of the reboiler and condenser in the feedforward-feedback cascade control system. To provide precise quantitative support, Table 4 summarizes the steady-state reconstruction data of key energy input nodes of the system before and after the feed composition disturbance and the final deviation magnitude.

Table 4. Steady-state reconstruction data and deviation index under feed composition disturbance

| Column ID | Initial Feed Fraction (wt%) | Disturbed Feed Fraction (wt%) | Initial Reboiler Duty (kW) | Compensated Reboiler Duty (kW) | Final Purity Deviation (%) |
|---|---|---|---|---|---|
| T101 | 35.2 | 30.2 (-5 percentage points) | 1580.2 | 1465.5 | -0.05 |
| T102 | 20.5 | 25.5 (+5 percentage points) | 1295.4 | 1410.2 | -0.08 |
| T103 | 25.1 | 20.1 (-5 percentage points) | 1850.6 | 1735.8 | -0.12 |
| T104 | 6.8 | 11.8 (+5 percentage points) | 960.5 | 1085.4 | -0.04 |

Table 4 lists the steady-state reconstruction data and deviation indices under feed composition disturbances. The disturbance reported in Table 4 denotes an absolute change of five percentage points in mass fraction rather than a five-percent relative change. The feed fractions of all four-columns were disturbed by ±5%, with T101 decreasing from 35.2% to 30.2%, T103 from 25.1% to 20.1%, T102 increasing from 20.5% to 25.5%, and T104 increasing from 6.8% to 11.8%. Correspondingly, the reboiler load was compensated, and the final purity deviation ranged from -0.04% to -0.12%, with T103 showing the largest deviation and T104 the smallest. The adaptive

control performance of the system under significant feed composition disturbances is shown in Figure 8.

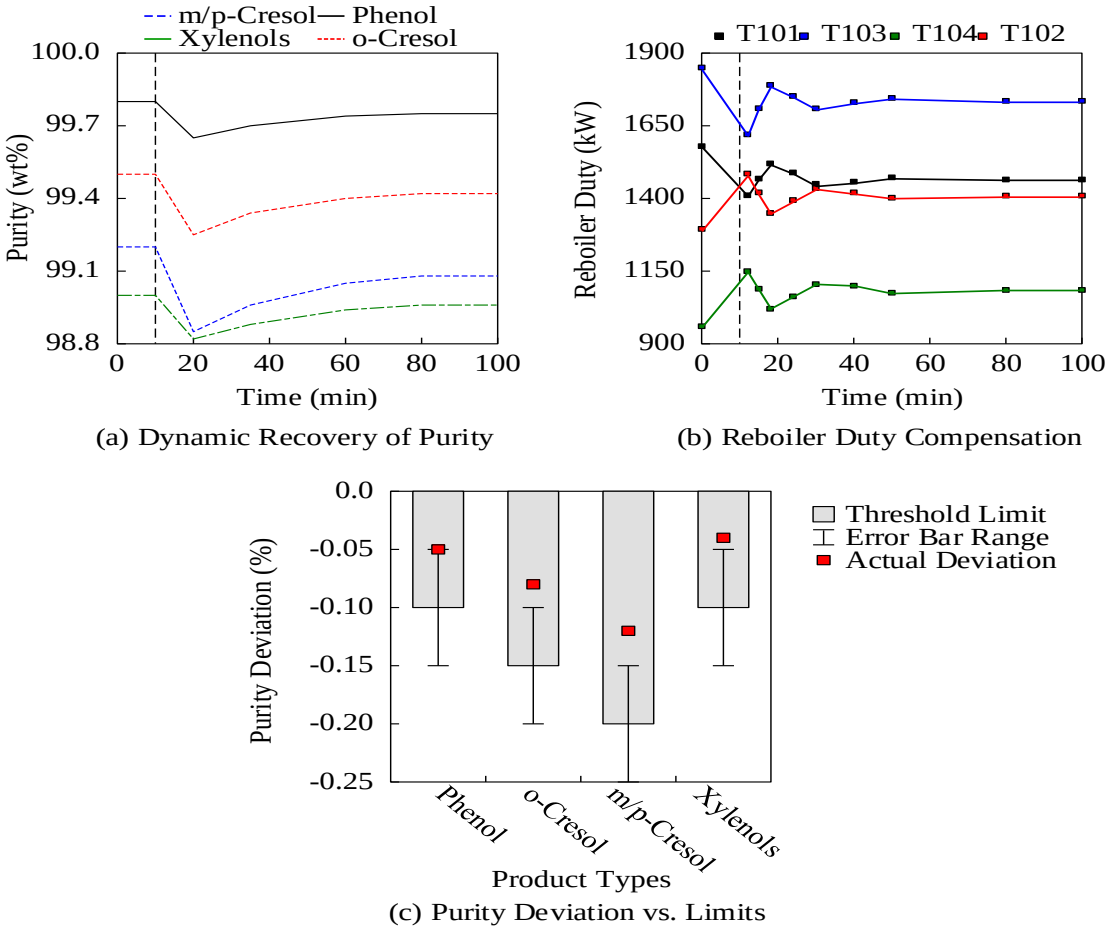


(a) Dynamic Recovery of Purity (b) Reboiler Duty Compensation

(c) Purity Deviation vs. Limits

Fig. 8. Control adaptive adjustment performance of the system under large disturbances in feed components

Figure 8(a) shows the purity recovery line graph. After the component mutation at the 10th minute, the purity of m/p-cresol once bottomed out to 98.85%, but all four purity curves were forcibly pulled up within 80 minutes and aligned with the new steady-state benchmark (99.08%). Figure 8(b) presents continuous reboiler-duty compensation trajectories. The T101 reboiler duty converged from 1580.2 to 1465.5 kW after transient oscillations. Figure 8(c) presents signed steady-state purity deviations and allowable limits. The largest deviation was -0.12% for m/p-cresol and remained within the corresponding limit. The actual absolute purity deviation of each product (maximum of -0.12% for m/p-cresol) was strictly limited within the corresponding bar chart safety tolerance boundary (e.g., -0.20%) and the allowable range of the error bar, eliminating the risk of long-term concentration back mixing caused by extreme fluctuations.

## 4. Conclusion

Traditional separation processes are insufficient to address the low product purity, high energy consumption, and poor stability arising from the close boiling points and high thermosensitivity of coal-tar-derived mixed phenolic homologues. Therefore, an advanced continuous four-columns vacuum distillation process based on the NRTL model was developed. A continuous four-columns vacuum distillation steady-state process based on a non-random dual-liquid model was developed. A separation sequence consisting of phenol, o-cresol, m-/p-cresol mixed fraction, and xylenols columns was constructed. Considering the system's strong multivariate coupling and large time-delay characteristics, a temperature-concentration cascade dynamic control framework with feedforward compensation was designed. Steady-state optimization results showed that when the comprehensive operating pressure was maintained at 18.0 kPa, high-temperature condensation

reactions could be suppressed, achieving a maximum annual net economic margin of US$1.585 million after deducting raw-material cost and the total annual cost of the four-columns process. The total annual cost of the m-/p-cresol column (T103) was reduced to USD 8.505 million, while the average tray separation efficiency of the phenol column (T101) reached 72.8%. Phenol, o-cresol, the m-/p-cresol mixed fraction, and xylenols achieved purities of 99.8%, 99.5%, 99.2%, and 99.0%, with recoveries of 99.1%, 98.7%, 98.2%, and 97.5%, respectively. Dynamic tests showed that the maximum product-purity deviation remained within 0.15%. Steady-state recovery required 40-65 min under positive or negative 10% step disturbances in feed flow and up to 80 min under an absolute five-percentage-point change in feed composition. The research has limitations such as insufficient pilot test verification and failure to consider the impact of trace impurities. For an anhydrous feed rate of approximately 12.0 t/h, a water content of 0.5-2.0 wt% would introduce an additional vaporization duty of approximately 40-160 kW in T101 and increase the molar load on the vacuum system by approximately 3%-12%. Therefore, the reported four-columns simulation results apply only to feed after dewatering and light-end removal. Future work will establish a pilot-scale calibration model, investigate heat-integration options, and integrate the feedforward cascade-control strategy into an industrial distributed control system for real-time validation. The research results can help increase the added value of coal chemical by-products and promote green development.

## References


[1] Wiratama IG, Kong ZY, Yang A, Saptoro A, Wong BT, Zheng J, et al. A comprehensive review of reactive-extractive distillation (RED) for production and recovery applications. Ind Eng Chem Res. 2025;64(26):12881-12907. https://doi.org/10.1021/acs.iecr.5c00782

[2] Guo XH, Hu L, Xu ML, Chen MX, Ma ZH, Li S, et al. Separation and analysis of oxygen-containing compounds in a Shaanxi middle/low-temperature coal tar. ACS Omega. 2023;8(9):8201-8209. https://doi.org/10.1021/acsomega.2c04625

[3] Wang J, Zhang ZX, Ge XY, Cao HT, Wei Y. Study on the thermodynamic properties of two quaternary ammonium salt-based deep eutectic solvents and their efficient extraction performance of phenol from model coal tar. J Chem Eng Data. 2025;70(10):3965-3975. https://doi.org/10.1021/acs.jced.5c00354

[4] Zhang CD, Shang WC, Zhang XN, Huang XL, Wang XY. Separation of m-/p-cresol in mixed phenols by complexation crystallization. Sep Sci Technol. 2025;60(8):1002-1012. https://doi.org/10.1080/01496395.2025.2466021

[5] Shiau LD. Purification of p-cresol, o-cresol, m-cresol, and 2,6-xylenol from the quaternary mixture by three-phase crystallization. Ind Eng Chem Res. 2023;62(20):8010-8020. https://doi.org/10.1021/acs.iecr.3c00711

[6] Lv Q, Ma Y, Yao Q, Sun M. A review on the extraction of phenols from coal tar: Composition distribution and analysis, methods and mechanism, process and industrialization prospect. Energy Fuels. 2025;39(3):1479-1506. https://doi.org/10.1021/acs.energyfuels.4c04060

[7] Guo J, Pan C, Feng B, Qiu X, Zhu Q, Song H, et al. Conceptual design and development of an environment-friendly process for simultaneous extraction of phenol and naphthalene compounds from tar. Ind Eng Chem Res. 2023;62(38):15553-15562. https://doi.org/10.1021/acs.iecr.3c01388

[8] Yang ZX, Hu DK, Wang Q, Hui YR, Wang YY, Li YR. Separation of phenolic compounds in coal tar by using deep eutectic solvent extraction with choline-urea: Based on phase equilibrium experiments and molecular mechanism investigation. J Chem Eng Data. 2025;70(1):456-469. https://doi.org/10.1021/acs.jced.4c00382

[9] Fonseca FG, Funke A. Modeling of liquid-vapor phase equilibria of pyrolysis bio-oils: A review. Ind Eng Chem Res. 2024;63(31):13401-13420. https://doi.org/10.1021/acs.iecr.4c00775

[10] Tang WT, Ward JD. Comparison of separation alternatives for two industrial C6-C7 aliphatic hydrocarbon mixtures including stacked complex sequences. Ind Eng Chem Res. 2022;61(36):13488-13504. https://doi.org/10.1021/acs.iecr.2c00756

[11] Yin M, Hua C, Lu P, Zhang H, Bai F. Design and control of pressure-swing heat integration distillation for the trichlorosilane purification process. ACS Omega. 2022;7(11):9254-9266. https://doi.org/10.1021/acsomega.1c05943

[12] Flores-Gómez LR, Gomez-Castro FI, Lopez-Villarreal F, Rico-Ramírez V. Assessment of the performance of fractional controllers on an extractive distillation column. Ind Eng Chem Res. 2025;64(24):12145-12155. https://doi.org/10.1021/acs.iecr.5c00037

[13] Qu Q, Zhang X, Shen Z, Chen M, Liu D, Sun J. Optimal control framework for alkane separation in semicontinuous distillation. Ind Eng Chem Res. 2023;62(40):16390-16400. https://doi.org/10.1021/acs.iecr.3c02020
[14] Qian X, Dang Q, Jia S, Yuan Y, Huang K, Chen H, et al. Operation of distillation columns using model predictive control based on dynamic mode decomposition method. Ind Eng Chem Res. 2023;62(50):21721-21739. https://doi.org/10.1021/acs.iecr.3c03275
[15] Guo L, Xu Q, Ma C, Shan B, Zhang F, Cui P, et al. Dynamic control design and performance evaluation of extractive distillation for N-hexane/acetone/chloroform. J Chem Technol Biotechnol. 2022;97(8):2114-2127. https://doi.org/10.1002/jctb.7083
[16] Zhang Q, Zhang S, Liu J, Li J, Liu J, Zhou J, et al. Catalytic upgrading of volatiles in co-pyrolysis of coal and biomass by Mo-MFI molecular sieves. RSC Adv. 2023;13(48):33852-33862. https://doi.org/10.1039/D3RA06925G
[17] Zhu JY, Wu YY, Wu B, Chen K, Ji LJ. Separation of m-cresol and p-cresol by NaZSM-5 with different Si/Al ratios. Environ Technol. 2024;45(19):3791-3806. https://doi.org/10.1080/09593330.2023.2231616
[18] Meng JQ, Wang C, Bai YH, Dong YC, Du J. Automatic design of extractive distillation sequence for a multicomponent azeotropic system. Ind Eng Chem Res. 2024;63(5):2294-2306. https://doi.org/10.1021/acs.iecr.3c03575
[19] Kang YY, Luo YQ, Yuan XG. Pseudo-transient modeling-assisted rigorous optimization of cyclic distillation considering tray hydraulics. Ind Eng Chem Res. 2023;62(25):9763-9772. https://doi.org/10.1021/acs.iecr.3c00741
[20] Pang HW, Forsuelo M, Dong XR, Hawtof RE, Ranasinghe DS, Green WH. Detailed multiphase chemical kinetic model for polymer fouling in a distillation column. Ind Eng Chem Res. 2023;62(36):14266-14285. https://doi.org/10.1021/acs.iecr.3c01461